

# Three-Step Segmentation of the Lower Airways with Advanced Leakage-Control

Silvia Born<sup>1</sup>, Dirk Iwamaru<sup>2</sup>, Matthias Pfeifle<sup>3</sup>, and Dirk Bartz<sup>1</sup>

<sup>1</sup> Visual Computing, ICCAS, Universität Leipzig, Germany

<sup>2</sup> CADMEI GmbH, Ingelheim, Germany

<sup>3</sup> Department of Neurosurgery, University Hospital Tübingen, Germany

**Abstract.** Segmentation of the tracheo-bronchial tree of the lung serves as an important tool for diagnosis and treatment planning of various pathologies, e.g. by allowing accurate volume measurements or detecting malformations. However, segmenting the airways of the human lung is notoriously difficult. This is due to the small size of the participating anatomical structures, which are moreover subject to partial volume and noise effects. Limited intensity contrasts between air and lung parenchyma also complicate segmentation. In this paper, we present our hybrid segmentation method consisting of three main steps, which are iterated until a satisfactory result is achieved. User interaction is limited to the specification of a seed point inside the easily detectable trachea. Further, we discuss the performance of our method within the EXACT09 challenge, where 20 test datasets with varying quality and pathologies had to be processed.

## 1 Introduction

Several pathologies can jeopardize a sufficient lung function. Among them are tumors, pulmonary embolism, collapse of the lungs (atelectasis), pneumonia, emphysema, asthma, and many more. For a proper diagnosis and treatment, the respective pathologies need to be identified and in some cases quantified. In the case of lung-surgery (i.e., for tumor treatment), this information is necessary for the intervention planning where the anatomical relation of diseased bronchi to non-diseased areas is required pre-operatively, i.e. to provide a safe distance to essential structures and to determine resectability.

The standard imaging method to gain anatomical information about lung parenchyma and airways is the computed tomography (CT). Segmenting e.g. the tracheo-bronchial tree from these datasets is difficult however. This is due to the small size of the anatomical structures of interest, the oftentimes low contrast between air and lung parenchyma, and the partial volume effect, which decreases this contrast further. Even today, airway segmentation is oftentimes carried out manually, especially in pathological cases with larger malformations. In the last years, a great number of (semi-)automatic methods have been presented in order to facilitate this tedious and time-consuming task (see Section 2). The main intention of the airway segmentation challenge EXACT09 is to give

the possibility to compare these segmentation methods in a meaningful manner (by applying them to the same 20 test datasets).

In this paper, we present our semi-automatic segmentation algorithm and discuss the results achieved within the EXACT09 challenge. The algorithm consists of three basic steps (3D region-growing, 2D wave propagation, and 2D template matching), which are iterated until the desired result is achieved. User interaction is limited to the specification of a seed point inside the easily detectable upper airways and in few cases the decision for a preprocessing step (filtering)<sup>4</sup>.

In the following parts of this paper, we briefly review related work in the field of airway segmentation in the next section. Afterwards, we will introduce the hybrid segmentation method, including all its pipeline stages in Section 3. After that, we present and discuss the results achieved within the EXACT09 challenge (Section 4). Finally in Section 5, we present conclusions and point to future research directions.

## 2 Related Work

Region growing algorithms are a common and frequently-used technique for airway segmentation [1–5]. Here, voxel with gray values within a pre-specified interval and connected to a seed point are included into the segmentation. Besides various advantages (fast, easy to apply), the main drawback is their sensitivity to leakages into the lung parenchyma. Various methods for leakage-avoidance have been presented. Filtering the CT dataset as pre-processing step is a straightforward corrective in this case, although this also implies loss of information on very small bronchi [2]. Gergel et al. introduced adaptive thresholds for leakage prevention with their 3D region growing approach. As soon as a leakage is detected, segmentation is continued with more conservative thresholds avoiding the leakage at that point [1]. Kitasaka et al. controlled leaking and bifurcation problems by a complex use of local volume of interest templates that limit the region growing area [3].

Further techniques used for airway segmentation apply mathematical morphologies [2, 6]. The whole CT dataset is searched for candidate airways with the help of several nonlinear filters. The final segmentation is generated by a reconstruction step that distinguishes correct from false candidates. Despite of the fact that no seed point selection is necessary, a further advantage is that airways, which are not directly connected to a seed point can be detected (useful for pathologic lungs). Main drawback of algorithms using mathematical morphologies is their long runtime.

Combining different methods in an airway segmentation pipeline is another successful approach. Kiraly et al. use a combination of an adaptive 3D region growing, 2D mathematical morphology, and an optional 2D median filter to increase the robustness of the segmentation algorithm while improving the quality of the results [2]. Law and Heng use a combination of region growing and center-line extraction to enhance the understanding of the 3D structure of the bronchial

---

<sup>4</sup> Other parameters are pre-defined and may be modified by the users.

tree [4]. Tschirren et al. introduced a segmentation based on fuzzy connectivity, i.e. voxels are detected as similar to seed voxels by fuzzy logics. Leakages are prevented by restricting the segmentation to a cylindrical-shaped ROI around bronchi [7]. Graham et al. deploy airway segmentation by detecting shorter bronchi sections, which are represented by surface meshes, and connecting them by interpolation. Strong filtering for the initial segmentation avoids leakages [8]. Finally, another hybrid solution is proposed by Mayer et al. [9], which is the basis for this contribution. It combines region growing with knowledge-based techniques and uses fuzzy logic for the segmentation of the bronchus walls.

### 3 Airway Segmentation Pipeline

The segmentation pipeline consists of three stages (Fig. 1). In the first stage, the trachea and central bronchi are segmented using standard 3D region growing methods.

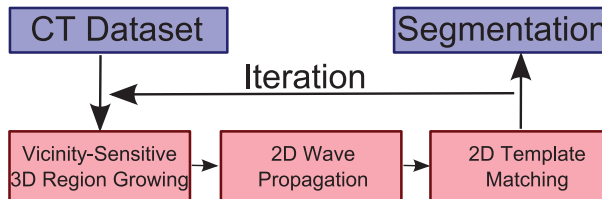
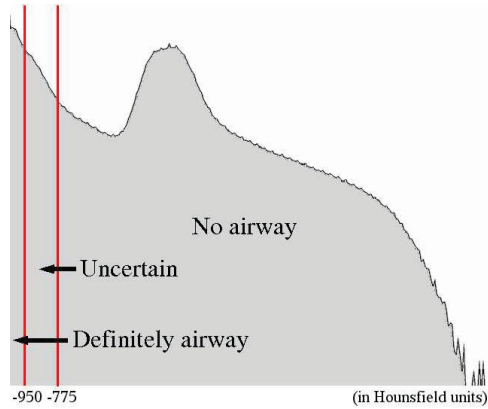


Fig. 1. Segmentation pipeline.

Partial volume effects and limited resolution of the CT scan (which essentially cause this effect) render this method as not satisfactory for segmentations of further generations of the bronchi, since bordering voxels cannot be sufficiently differentiated from tissue voxels. Therefore, a 2D wave propagation is initiated to complete the upper and central branches. Finally, a 2D template matching procedure is used to segment small lumen, which might be only a single voxel large. A feedback loop of the whole pipeline repeats the stages until no meaningful additions can be made to the previous segmentation (Fig. 1). Figure 5 shows the final results of five iterations. However, some datasets might require up to 15 iterations.

#### 3.1 Vicinity-Sensitive 3D Region Growing

The intensity values of CT dataset of the thorax can be divided into three categories (Fig. 2). Values below -950 Hounsfield units (HU) can be classified as **definitely airway** and values above -775 HU as **non-airway**. Voxels with values in between (in the isovalue interval from -950 HU to -775 HU) can belong



**Fig. 2.** Logarithmic histogram of CT thorax dataset.

to airway or tissue. They are classified as **uncertain** and need to be investigated further.

Based on this analysis, the 3D region growing algorithm extracts all voxels which are definitely airway, starting at the user-defined seed point in the trachea. To prevent the leaking into the parenchyma of the lungs in smaller airways (i.e., in emphysema), we use a masking technique from texture analysis; if the average gray value of a  $3 \times 3 \times 3$  voxel cube centered at the current voxel is within the save range (below -950 HU), we consider this voxel as being part of the airway. Otherwise, the respective voxel is not classified as airway in this stage. While this masking technique prevents leakage, it also impedes the segmentation of smaller bronchi. However, we usually accomplish the segmentation of the bronchial tree up to the fifth generation, whereas the bordering voxels are often not included, since their voxel values belong to the uncertain voxel value interval (see Fig. 3 and Fig. 5a/b). In the second iteration of the segmentation pipeline, the 3D region growing algorithm runs with the same threshold on the bordering voxels of the previously selected voxels.

### 3.2 2D Wave Propagation

Starting from segmented voxels of the previous step, 2D wave propagation tries to reconstruct bronchi walls within a single CT slice. It starts at each boundary voxel of the airway voxels from 3D region growing and propagates waves to detect the walls of the bronchi (Fig. 3b). Voxels at position  $X$  in the **uncertain** areas are classified by fuzzy logic rules that consider the density value  $V(X)$  (in Hounsfield units), the largest local  $N_4$  neighborhood (in 2D) gradient  $G(X)$ , and if voxels in the local  $N_4$  neighborhood are already classified as wall pixels

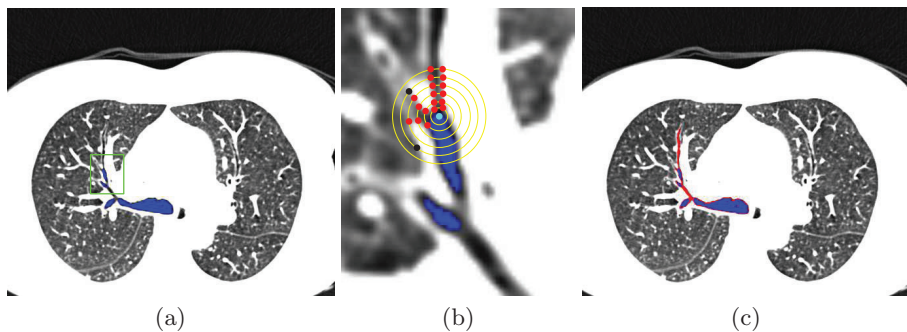


**Fig. 3.** Completion of bronchi walls; (a) shows the result of the 3D region growing (blue). The green rectangle marks the zoomed area shown in (b). (b) shows the wave propagation in progress. The cyan boundary voxel is chosen as starting point. The yellow circles mark the propagated waves and the red points mark the airway candidate voxels. The black points failed the leaking test, since the number of voxels of that wave was increasing too fast. Note that the actual waves have a Rhombus-like shape, driven by the N4-neighborhood. (c) shows the completion of that segmentation by 2D wave propagation (red). The voxels (within the body) in the iso-range of **definitely airway** are marked in blue, of the **uncertain** range in black/grey, and of the **no airway** range in white.

(no airway) in a previous wave  $W(X)$ :

$$f_{wave}(X) = c_v * V(X) + c_g * G(X) + c_w * W(X), \quad (1)$$

with  $c_v = 1, c_g = 1, c_w = 0.75$ .

where  $V(X)$  and  $G(X)$  are mapped into the closed interval  $[1.0, 0.0]$ , and  $W(X)$  is either 1 – if there is a classified wall pixel in the N4 neighborhood – or 0 – otherwise. Essentially, if  $f_{wave}(X) \geq c_{wall}$ , the voxel is classified as wall<sup>5</sup>.

Critical to the wave propagation is the evaluation of the classified airway areas, if they really belong to the airways. To achieve this goal, the additional voxels segmented by each wave are monitored by a protocol that verifies the shape and size of each bronchus candidate, using a set of default parameters (Fig. 3b). As metric, we count the number of voxels selected by the  $n$  waves propagating within a plane ( $BPS_n$  for BronchusPlaneSize), and the wave diameter ( $WD_n$ ) of the current wave  $n$  as the number of selected voxels of wave  $n$ . Furthermore, we define the average number of voxels of the first  $n$  waves ( $AWD_n$  for Average Wave Diameter).

Segments of the tracheo-bronchial tree are identified by sequences of as airway classified voxels in a wave. Figure 3b shows two sequences marked by the red points, thus depicting a bifurcation. The shape rules essentially assume that no wave detects segment splits in more than two subsequent segments at a bifurcation. A third segment (of not yet selected voxels) in one 2D wave propagation

<sup>5</sup> Typically,  $c_{wall} = 1.74$ .

test (in one slice) is henceforth considered as leakage into the lungs and is considered invalid. At each bifurcation, the segment identification process starts again recursively.

As closer examination of previously examined CT thorax datasets showed, two very close bifurcations were never located close enough to be detected as a third segment by the 2D wave propagation, thus they were not falsely identified as leakage.

$$WD_n > d_{max} \quad (2)$$

$$WD_n / WD_{n-1} > d_{WD_{ratio}} \quad (3)$$

$$BPS_n > d_{size} \quad (4)$$

$$AWD_n - AWD_{n-1} > d_{AWD_{current}} \quad (5)$$

$$AWD_{max} - AWD_{min} > d_{AWD_{longterm}} \quad (6)$$

The size rules limit the growing of the wave propagation<sup>6</sup>. If the diameter of a bronchi candidate exceeds a certain size (Equation 2), or if the wave diameter is increasing too fast from the previous wave (Equation 3, see also black points in Fig. 3b), the respective segment recursion is terminated and the results are considered as leakages (invalid). Furthermore, if candidates grow spontaneously (while shrinking before) or the overall in plane voxel size  $BPS_n$  of the candidate becomes unrealistically large (Equation 4), the recursion is again terminated and the results are set to leakages (invalid). The last two rules (Eqn. 5 and 6) test the current and long-term growth of the wave front. Specifically, they test if the segments are shrinking (as assumed) or growing. The protocol starts testing after the first three waves, since they frequently show an unstable behavior. During the wave propagation, all invalid results are removed from the segmentation. However, initial correct results (i.e., for the first  $p$  waves) are preserved.

To follow a bronchus through several slices, virtual waves are propagated in neighboring slices. If one of these virtual waves is similar to the shape and size of the wave propagation in the current slice, another recursive wave propagation in the neighboring slice is initiated. Specifically, the recursive testing of waves in neighboring slice is initiated only for no-branching segments that have classified wall elements from 2D wave propagation. Furthermore, these wall elements may only differ by one voxel to the wall elements of the new neighboring slice segment.

Similar to the first step of the pipeline, 2D wave propagation uses almost the same parameters in the subsequent iteration; only the peripheral bronchi diameter is reduced since the lower airways (higher generations) only grow smaller.

### 3.3 2D Template Matching

Without the used careful validity testing, the previous two stages would leak into the surrounding area, if the airways become too small to be picked up,

<sup>6</sup> We use  $d_{max} = 6.1mm$ ,  $d_{WD_{ratio}} = 1.75$ ,  $d_{size} = 500mm^2$ ,  $d_{AWD_{current}} = 1.13$ ,  $d_{AWD_{longterm}} = 3.0$ .

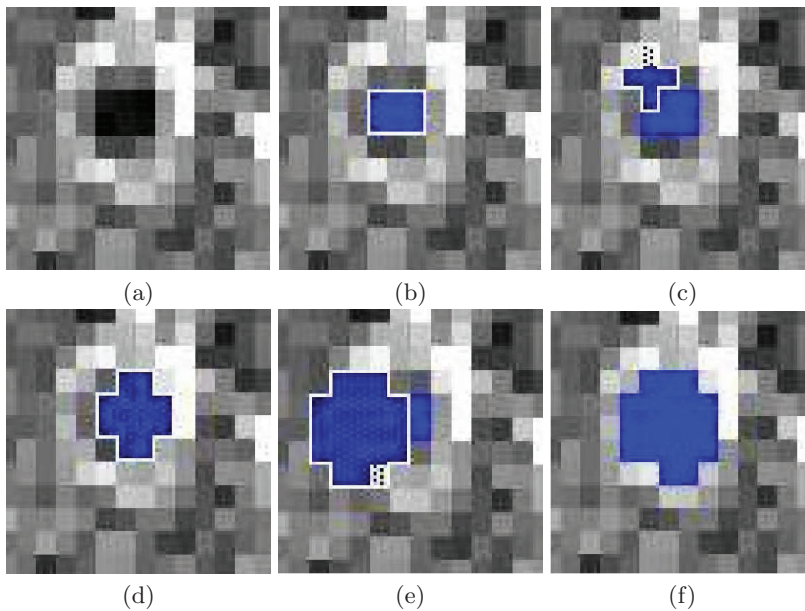


**Fig. 4.** Template matching: (a) shows a peripheral airway. 2D seeding is started on pixels of the category **uncertain**. The result is marked blue (b). From there the seeding area templates (white polygon with black dot pattern) are formed and tested on different locations around the seeding. The seeding is repeated on the category uncertain and template (marked by a pattern, (c) to (e)). (f) shows the best result after the classification.

in particular in areas where the airways might have the size of only one voxel. To select these voxels, but still prevent the leaking, we apply a 2D template matching technique that evaluates the candidate area below templates with the isovalue category **uncertain** (between -950 HU and -775 HU). This stage is organized in two steps; the first step establishes templates that are used in the second step to evaluate the local voxel neighborhood.

First, 2D template matching applies 2D region growing starting from the boundary voxels of the previous segmentations (Fig. 4). The thresholds are varied – from the upper threshold of the **uncertain** isovalue interval (-775 HU) – until the number of selected voxels is below the critical limit (i.e., 35 voxels), since it can be assumed that they did not leak out. Based on this selected voxel area, circular templates of varying sizes are generated.

In the second step, we apply a 2D region growing and use the templates to differentiate the thresholds; below the template, we are using the upper **uncertain** threshold (-775 HU), while we are using the original template threshold outside of the template. By moving the templates over the local area, we generate various segmentation candidates (see Fig. 4b-e) which are again evaluated by a set of fuzzy rules. This time, we consider the average density value  $\bar{V}(X)$  of

the template area and the average (gradient range is clamped in order to reduce data artifacts) gradient  $G(X)$  to the surrounding voxels in the N8 neighborhood (within a single slice). The best possible result is then selected and added to the segmentation (Fig. 4 and Fig. 5d).

$$f_{template}(X) = c_{ave} * \bar{V}(X) + c_{grad} * G(X), \quad (7)$$

*with  $c_{ave} = 0.25$  and  $c_{grad} = 0.75$ .*

Here,  $\bar{V}(X)$  is mapped from  $[-1000, -775]$  to  $[0.0, 1.0]$ , and  $G(X)$  is mapped into the range  $[0.0, 1.0]$ . Illustratively, this means that accepted candidates have a low average density value and a high boundary contrast. The candidate with the largest  $f_{template} \geq 0.7$  (Eqn. 7) is accepted as airway (Fig. 4f and Fig. 5d). However, if the size of the template controlled area is larger than twice as much as for the previous slice, a leak-out is assumed, thus the area of the current slice is assumed invalid.

In the subsequent iterations, voxels which have already been unsuccessfully tested for inclusion, are excluded from template matching. This is mainly to save time – 2D template matching is the single most time consuming stage of the segmentation pipeline – and they usually do not contribute in later iterations.

## 4 Application to EXACT09 datasets

When applying our semi-automatic segmentation method, user interaction is required for setting the seed point in the trachea. All parameters (thresholds, propagation diameter, etc.) are pre-specified. These default parameters (see Section 3), which were fixed based on previously segmented CT datasets and validated with the provided training data, also worked very well with the majority of the test datasets. An optimization of the parameters for individual datasets is possible, but improves the segmentation results only slightly compared to the standard setting. We consider this as stability feature of our approach.

In several cases, we faced the problem that due to noise effects (especially in low-dose CT datasets), the initial vicinity-sensitive 3D region-growing showed no satisfying results. A slight adjustment of the segmentation thresholds might solve this problem (as e.g. in case 26). However, these thresholds are based on expert knowledge, so increasing these parameters too much easily leads to false positives, when uncertain or tissue voxels are classified as airway. Thus, in these cases a preprocessing step, i.e. the application of a gentle Gaussian filter (kernel size of 3 voxels), was included into the pipeline. Although filtering also implicates a loss of information concerning the lower and smaller bronchi, it turns out to be the better choice than adjusting thresholds, risking leakages, and thereby a higher false positives rate. Altogether, this pre-processing step allowed fairly good segmentations compared to the problems that arose before.

The segmentation results were evaluated according to two main categories: the overall segmentation result and the leakage robustness (see Table 1). Concerning the segmentation sensitivity, our method detected 41.7% of the branches

**Table 1.** Evaluation measures for the twenty cases in the test set.

	Branch count	Branch detected (%)	Tree length (cm)	Tree length detected (%)	Leakage count	Leakage volume (mm <sup>3</sup> )	False positive rate (%)
CASE21	64	32.2	35.5	32.1	0	0.0	0.00
CASE22	144	37.2	98.9	29.9	0	0.0	0.00
CASE23	158	55.6	112.3	43.1	5	89.8	0.70
CASE24	112	60.2	83.4	51.3	2	8.2	0.04
CASE25	151	64.5	110.5	43.8	4	50.7	0.21
CASE26	54	67.5	38.4	58.4	3	297.1	4.85
CASE27	52	51.5	35.7	44.0	0	0.0	0.00
CASE28	89	72.4	63.2	57.6	0	0.0	0.00
CASE29	58	31.5	36.1	26.2	0	0.0	0.00
CASE30	98	50.3	67.6	44.2	1	1.8	0.03
CASE31	61	28.5	38.6	22.0	1	6.7	0.08
CASE32	64	27.5	46.8	21.5	2	108.6	0.93
CASE33	55	32.7	38.4	26.1	0	0.0	0.00
CASE34	139	30.3	84.8	23.7	4	37.6	0.20
CASE35	180	52.3	117.2	37.9	13	155.4	0.93
CASE36	69	19.0	60.8	14.7	0	0.0	0.00
CASE37	53	28.6	43.0	24.2	0	0.0	0.00
CASE38	40	40.8	30.6	46.1	0	0.0	0.00
CASE39	101	19.4	78.9	19.3	0	0.0	0.00
CASE40	127	32.6	93.4	24.1	3	28.6	0.20
Mean	93.5	41.7	65.7	34.5	1.9	39.2	0.41
Std. dev.	43.0	16.2	29.6	13.2	3.1	74.8	1.09
Min	40	19.0	30.6	14.7	0	0.0	0.00
1st quartile	55	28.6	38.4	23.7	0	0.0	0.00
Median	79	35.0	62.0	31.0	1	0.9	0.01
3rd quartile	144	60.2	98.9	46.1	4	89.8	0.70
Max	180	72.4	117.2	58.4	13	297.1	4.85

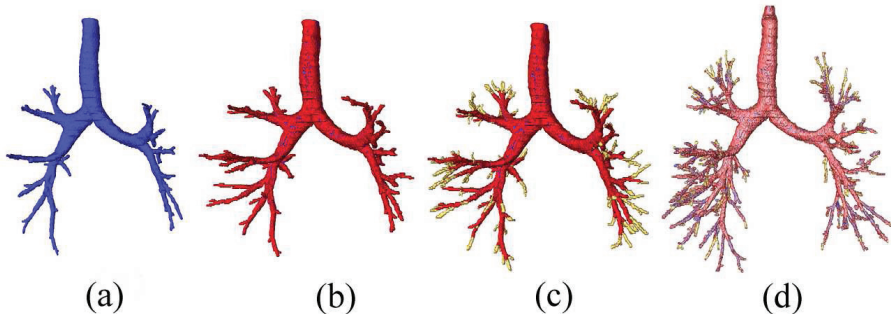


**Fig. 5.** Three segmentation stages: (a) region growing, (b) wave propagation, (c) template matching, (d) final segmentation result

and 34.5% of the tree length (length of the centerlines of detected branches). Both compared to the gold standard, which is the airway segmentation result carried out manually by radiologists and other medical experts. With that, our method belongs to the lower midrange, when compared to all other 14 algorithms, and ranks second in the group of semi-automatic methods. A problem reducing the sensitivity of our method, were larger gray values occurring in the bronchi due to pathologies (e.g. caused by secretion). These voxel are then classified as lung parenchyma and interrupt the segmentation (see Figure 6).

The strength of our algorithm, however, is leakage-control. Only 0.41% of the detected branches were false positives (in Table 1 referred to as *false positive rate*) and with that result we achieved rank three in total. The positive predictive value, which measures the accuracy that existing branches are detected (correctly found bronchi branches / (correctly found bronchi branches + found false positive bronchi branches)), is 98.0% and in 50% of our segmentations, no leakage occurred at all.

In the segmentation of airways in CT datasets, a satisfying trade-off between detecting a maximal number of bronchi and avoiding leakages has to be found. The evaluation within the EXACT09 challenge shows, that our segmentation method belongs to the more conservative techniques, where leakage-avoidance has a very high priority.

As noted before, usually five to seven iterations are sufficient for a segmentation of the tracheo-bronchial tree. Overall, this corresponds to a typical segmentation duration between 10 and 30 seconds on a PC with a Intel Core 2 Duo processor, each core running at 2.4 GHz.

## 5 Conclusions and Future Work

In this paper, we presented a semi-automatic segmentation method with a pipeline of three main steps, which is iteratively applied. These main steps are 3D region-

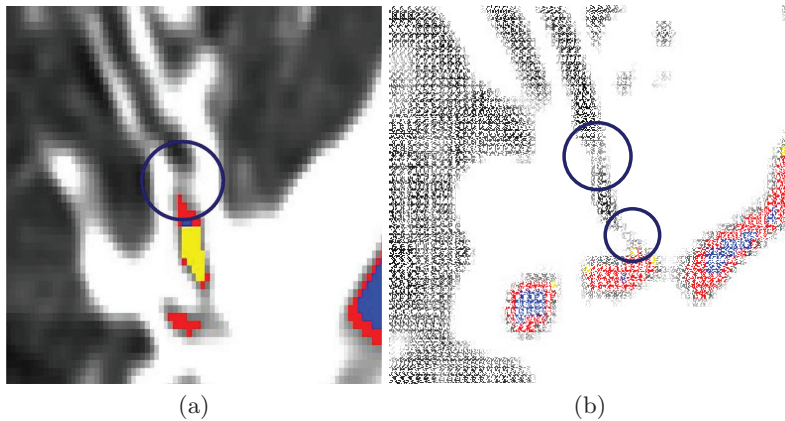


**Fig. 6.** Areas with higher gray values (marked by circles) inside the bronchi interrupt the segmentation. Examples from Case36 (a) and Case39 (b).

growing, 2D wave propagation, and 2D template matching, all of which are implemented with special focus on leakage-prevention (see Section 3). The results within the EXACT09 airway segmentation challenge justify this effort with a very low false positive rate and a small leakage volume. The drawback of the powerful leakage-control is, however, the reduced sensitivity concerning the overall segmentation performance.

A straightforward advancement of our method is stepping from 2D to 3D for the wave propagation and the template matching. At present, these two pipeline stages work on individual slice images. Thus, detecting bronchi located orthogonal to these slices is usually not possible within the same iteration. It turned out, that the subsequent vicinity-sensitive 3D region growing – followed by the other 2D pipeline stages – is able to compensate for this effect in many cases. Hence, implementing 3D wave propagation and 3D template matching will primarily show an improvement concerning runtime (by achieving the same result in fewer iterations), but beyond that we also expect some better identification of smaller bronchi.

## References

1. Gergel, I., Wegner, I., Tetzlaff, R., Meinzer, H.P.: Zweistufige Segmentierung des Tracheobronchialbaums mittels iterativen adaptiven Bereichswachstumsverfahren. In: Proc. of Workshop Bildverarbeitung für die Medizin. (2009) 56–60
2. Kiraly, A., Higgins, W., McLennan, G., Hoffman, E., Reinhardt, J.: Three-Dimensional Human Airway Segmentation Methods for Clinical Virtual Bronchoscopy. *Academic Radiology* **9**(10) (2002) 1153–1168

3. Kitasaka, T., Mori, K., Hasegawa, J., Toriwaki, J.: A Method for Extraction of Bronchus Regions from 3D Chest X-ray CT Images by Analyzing Structural Features of the Bronchus. *Forma* **17**(4) (2002) 321–338
4. Law, T., Heng, P.: Automatic Centerline Extraction for 3D Virtual Bronchoscopy. In: Proc. of MICCAI. Volume 1935. (2000) 786–795
5. Mori, K., Hasegawa, J., Suenaga, Y., Toriwaki, J., Anno, H., Katada, K.: Automated Labeling of Bronchial Branches in Virtual Bronchoscopy System. In: Proc. of MICCAI. Volume 1496. (1998) 870–878
6. Fetita, C., Preteux, F., Beigelman-Aubry, C., Grenier, P.: Pulmonary Airways: 3-D Reconstruction from Multislice CT and Clinical Investigation. In: IEEE Trans. on Medical Imaging. Volume 23. (2004) 1353–1364
7. Tschirren, J., Hofmann, E., McLennan, G., Sonka, M.: Intrathoracic Airway Trees: Segmentation and Airway Morphology Analysis From Low-Dose CT Scans. In: IEEE Trans. on Medical Imaging. (2005) 1529–1539
8. Graham, M., Gibbs, J., Higgins, W.: Robust System for Human Airway-Tree Segmentation. In: Proc. of SPIE Medical Imaging. Volume 6914. (2008) 69141J
9. Mayer, D., Bartz, D., Fischer, J., Ley, S., del Rio, A., Thust, S., Kauczor, H.U., Heussel, C.P.: Hybrid Segmentation and Virtual Bronchoscopy Based on CT Images. *Acad Radiol* **11** (2004) 551–565